

# Signature of the microcavity exciton polariton relaxation mechanism in the polarization of emitted light

Georgios Roumpos,<sup>1,\*</sup> Chih-Wei Lai,<sup>1,2</sup> T. C. H. Liew,<sup>3</sup> Yuri G. Rubo,<sup>3,4</sup> A. V. Kavokin,<sup>3,5</sup> and Yoshihisa Yamamoto<sup>1,2</sup>

<sup>1</sup>*E. L. Ginzton Laboratory, Stanford University, Stanford, CA, 94305, USA*

<sup>2</sup>*National Institute of Informatics, Hitotsubashi, Chiyoda-ku, Tokyo 101-8430, Japan*

<sup>3</sup>*School of Physics and Astronomy, University of Southampton, Highfield, Southampton SO17 1BJ, UK*

<sup>4</sup>*Centro de Investigación en Energía, Universidad Nacional Autónoma de México, Temixco, Morelos, 62580, Mexico*

<sup>5</sup>*Marie-Curie Chair of Excellence “Polariton devices”,  
University of Rome II, 1, via della Ricerca Scientifica, Rome, 00133, Italy*

(Dated: March 5, 2019)

We have performed real and momentum space spin-dependent spectroscopy of spontaneously formed exciton polariton condensates for a non-resonant pumping scheme. Under linearly polarized pump, our results can be understood in terms of spin-dependent Boltzmann equations in a two-state model. This suggests that relaxation into the ground state occurs after multiple phonon scattering events and only one polariton-polariton scattering. For the circular pumping case, in which only excitons of one spin are injected, a bottleneck effect is observed, implying inefficient relaxation.

PACS numbers: 78.67.De, 03.75.Nt, 78.70.-g

Bose-Einstein condensation (BEC) is an active field of research, especially after its realization in dilute alkali gases [1, 2]. Microcavity exciton polaritons [3, 4, 5], composite quasi-particles consisting of quantum well (QW) exciton and microcavity photon components, have been proposed as candidates for BEC [6]. Due to their low mass, the critical temperature for BEC is expected to be high, even up to room temperature [7]. The confinement in two dimensions, along with the dual exciton-photon character of polaritons, enables interesting optical studies. Indeed, several characteristic signatures of dynamical condensation have been reported in recent years [8, 9, 10].

However, the lifetime of polaritons is short, on the order of 10 psec in our GaAs-based sample when condensation is observed, so the system is inherently dynamical. In previous studies, the final energy distribution of polaritons was compared to the Bose-Einstein distribution for steady-state [9] or time-resolved [11] data. These results are explained by modeling the relaxation mechanism in terms of polariton-acoustic phonon and polariton-polariton scattering [12, 13, 14]. However, taking into account the polariton spin degree of freedom introduces further complications, due to the interplay between energy and spin relaxation [15, 16, 17].

Here, we report the insights we gained on the relaxation mechanism, based on polarization-dependent studies of exciton polariton condensation under non-resonant incoherent pumping. For linearly polarized pump, the condensate emission develops both non-zero linear and circular polarization. We observed rotation of the linear polarization axis by  $\sim 90^\circ$  between the pump and condensate. The exact rotation angle is correlated with the handedness of the observed circular polarization. These signatures are similar to the observations of a parametric oscillator experiment [18], which were interpreted [19] in

terms of spin-asymmetric polariton-polariton interaction [20, 21, 22]. We use a two-state model employing the spin-dependent Boltzmann equations [16] to understand our experimental results. The agreement we obtain reveals the similarities of the non-resonant pumping scheme to parametric oscillator (magic angle) geometries [23]. In the former case, it is believed that polaritons suffer multiple scatterings with phonons and other polaritons before reaching the  $k_x \sim 0$  region, so any phase coherence inherited from the laser should be lost, whereas in the latter case only one polariton-polariton interaction occurs [24]. Further, the observed spectra under circular pumping, show a bottleneck effect. This suggests that polaritons cannot efficiently relax into the ground state when only one spin species is present. A similar suppression of the scattering rate was observed in parametric amplification experiments [25, 26].

The sample and spectroscopy setup is the same as described in Ref. [27]. Our setup allows us to perform near field (NF - real space) and far field (FF - momentum space) imaging and spectroscopy. The measurements reported here are taken from a spot on the sample with photon-exciton detuning  $\delta = +6\text{meV}$ , while the Rabi splitting is  $2\hbar\Omega_{\text{Rabi}} = 14\text{meV}$ . The sample is kept at a temperature of  $7 - 8\text{K}$  on the cold finger of a He flow cryostat. The system is pumped with a mode-locked Ti:Sapphire laser of 2psec pulse width and 76MHz repetition rate focused on an ellipse of diameters  $50\mu\text{m}$  and  $30\mu\text{m}$ . For FF data, luminescence is collected through an aperture at the first image plane corresponding to a circular area of  $30\mu\text{m}$  diameter on the sample. The pumping laser is incident at an angle of  $55^\circ$  (Fig. 1 inset, corresponding wavenumber  $k_y = -7\mu\text{m}^{-1}$ ), at the exciton resonance wavelength. The setup employs liquid crystal polarization components as shown on Fig. 1. We can pump with

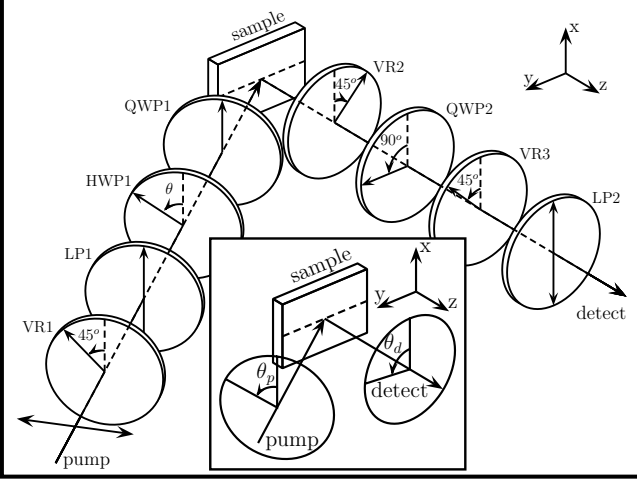


FIG. 1: The polarization measurement setup. Vectors label the fast or polarization axes of the optical components. The laser pump is initially horizontally polarized ( $\theta_p = 90^\circ$ ), and is incident at an angle of  $55^\circ$  with respect to the growth direction  $z$ . Luminescence is collected along the  $z$ -axis. The first variable retarder (VR1) and linear polarizer (LP1) work as a variable attenuator. By rotating a half waveplate (HWP1), and by using a removable quarter waveplate (QWP1), we can implement various polarization states for the pump. The second variable retarder (VR2) is used as a zero, half, or quarter waveplate. The combination of a quarter waveplate (QWP2), variable retarder (VR3) and linear polarizer (LP2) is used for detection of a particular linear polarization state, depending on the retardance of VR3. Inset: Definition of angles  $\theta_p$  and  $\theta_d$  corresponding to the polarization axes of the pump and detection respectively.

linear polarization of varying angle  $\theta_p$ , as well as general elliptical polarization. The detection can be performed for linear polarization of arbitrary angle  $\theta_d$ , or for right- and left-circular polarization.

Using the transfer matrix method [28, 29] for exciton inhomogeneous broadening of  $3meV$ , as measured at the far blue detuned regime, we estimate that the absorbed laser power for TM ( $\theta_p = 90^\circ$ ) and TE ( $\theta_p = 0^\circ$ ) pumping is  $\sim 4\%$  and  $\sim 0.9\%$  respectively of the incident power. We assume that the absorption efficiency is independent of power. In the rest of the paper, the various pump polarization states refer to the actually absorbed light inside the cavity, taking into account the calculated differential absorption of TM and TE pumping.

A ground state ( $k_{x,y} = 0$ ) linear polarization splitting of  $\sim 50\mu eV$ , similar to earlier studies [18, 30, 31], is measured for low excitation power and the current sample orientation, possibly due to crystal asymmetry. The observed superimposed linear polarization splitting for  $k_x \neq 0$  is in quantitative agreement with a transfer matrix calculation.

The polarization state of light is characterized by the following three parameters (normalized with respect to

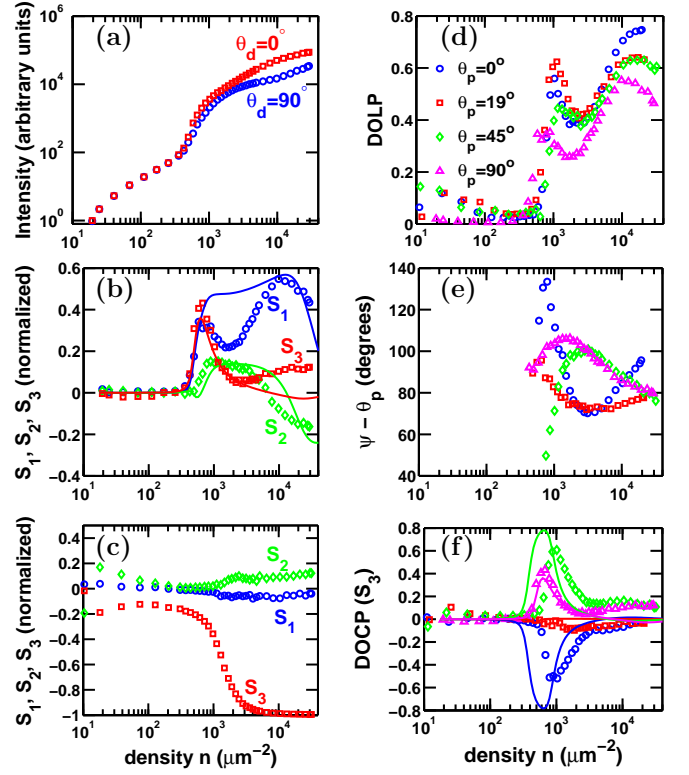


FIG. 2: (color) Measurement of Stokes parameters (markers) compared with the theoretical model (solid lines). (a) Horizontal pumping ( $\theta_p = 90^\circ$ ). Collected luminescence for  $\theta_d = 0^\circ$  (red squares) and  $\theta_d = 90^\circ$  (blue circles) vs. injected particle density in  $\mu m^{-2}$  per pulse per QW. A clear threshold is observed at  $5 \times 10^2 \mu m^{-2}$ . (b-c) Degree of polarization measurement for (b)  $\theta_p = 90^\circ$  linear pumping and (c) left circularly polarized pumping. Blue circles:  $S_1$ , green diamonds:  $S_2$ , red squares:  $S_3$  defined in eq. (1). (d-f) Calculated polarization parameters from the measurement of the Stokes parameters for linear pumping (eqs. (1-2)). (d) DOLP. (e) Angle for major axis of linear polarization  $\psi$  relative to  $\theta_p$ . (f) Degree of circular polarization ( $S_3$ ).

the total power), which are equivalent to the Stokes parameters as originally defined [32]:

$$S_1 = \frac{I_{0^\circ} - I_{90^\circ}}{I_{0^\circ} + I_{90^\circ}}, \quad S_2 = \frac{I_{45^\circ} - I_{-45^\circ}}{I_{45^\circ} + I_{-45^\circ}}, \quad S_3 = \frac{I_L - I_R}{I_L + I_R}. \quad (1)$$

$I_{0^\circ}$ ,  $I_{90^\circ}$ ,  $I_{45^\circ}$ , and  $I_{-45^\circ}$  are the intensities of the linearly polarized components at  $\theta_d = 0^\circ, 90^\circ, 45^\circ$ , and  $-45^\circ$  respectively.  $I_L$  and  $I_R$  are the intensities of the left- and right-circularly polarized components respectively. From the above parameters, we can calculate the degree of linear polarization (DOLP) and the angle of the major linear polarization axis  $\psi$

$$\text{DOLP} = \sqrt{S_1^2 + S_2^2}, \quad \psi = \frac{1}{2} \arctan \left( \frac{S_2}{S_1} \right). \quad (2)$$

We record the far field spectra for varying pumping power and polarization angles  $\theta_p$  and  $\theta_d$ , and sum the

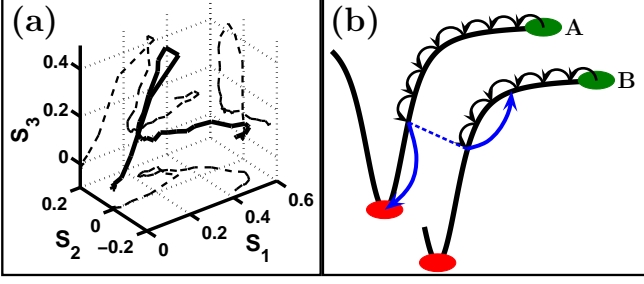


FIG. 3: (color) (a) The path followed by the polarization vector for increasing excitation power ( $\theta_p = 90^\circ$  linearly polarized pumping). The projections on the three normal planes are shown with thin dashed lines. (b) Schematic of the proposed relaxation mechanism: the optically excited polariton A, first loses energy by phonon scattering, then scatters with one other polariton (B) and populates the ground state.

intensities inside the area  $|k_x| < 0.55 \mu\text{m}^{-1}$  (corresponding to  $4^\circ$ ). The observed normalized intensities  $I_{\theta_d}$  are only weakly dependent on the choice of this area, and are shown in Fig. 2. For circularly polarized pump (Fig. 2(c)) and well above threshold, the signal is perfectly circularly polarized, up to  $-99.4\%$ . This is due to the short polariton lifetime ( $\sim 10\text{ps}$ ), which is shorter than the spin relaxation time. The negative sign of  $S_3$  means that the angular momentum of the emitted photons along the  $z$ -axis is the same as that of the optically injected exciton polaritons. For linear pumping above threshold, a non-zero degree of linear polarization develops (Fig. 2(d)), the polarization axis being rotated by  $\sim 90^\circ$  compared to the pump (Fig. 2(e)). Also, a circularly polarized component emerges, while  $S_3$  changes sign for varying  $\theta_p$  (Fig. 2(f)). The sign change is correlated with the deviation of  $\psi - \theta_p$  from  $90^\circ$ . The path followed by the polarization vector for increasing power and  $\theta_p = 90^\circ$  linearly polarized pumping is plotted in Fig. 3(a).

To interpret these results we have used a simplified model based on the spin-dependent Boltzmann equations for polaritons in microcavities [16]. Our model is based upon two states, representing the condensate and reservoir, each characterized by a  $2 \times 2$  spin density matrix. The polariton-polariton scattering matrix element in parallel spin configuration,  $\alpha_1$  (positive), is believed to be much greater in magnitude [19, 20] than that in antiparallel configuration,  $\alpha_2$  (negative). Therefore, calculating the transition rates we keep only terms  $\propto \alpha_1^2$  and the interference terms  $\propto \alpha_1 \alpha_2$ . We assume the reservoir is quickly populated by the pump from fast polariton-phonon relaxation. Then we consider the polariton-polariton scattering processes, which populate the condensate (Fig. 3(b)).

The spin-anisotropy of the polariton-polariton interactions gives rise to two important effects. First, a  $90^\circ$  rotation of the linear polarization appears upon one polariton-polariton scattering, which has been evidenced

in parametric oscillator experiments in magic angle [18] as well as degenerate configurations [33]. This is because of the difference between the scattering matrix elements of linearly polarized polaritons

$$\langle \phi, \phi | V | \phi, \phi \rangle = \frac{1}{2} (\alpha_1 + \alpha_2), \quad (3)$$

$$\langle \phi + 90^\circ, \phi + 90^\circ | V | \phi, \phi \rangle = \frac{1}{2} (\alpha_1 - \alpha_2). \quad (4)$$

$V$  is the polariton-polariton interaction operator, and  $|\phi\rangle$  is the linear superposition  $\frac{1}{\sqrt{2}} (|\uparrow\rangle + e^{2i\phi} |\downarrow\rangle)$  of spin-up and spin-down polaritons. We note that if multiple polariton-polariton scattering events are involved, the initial polarization information should be lost. Second, if there is an imbalance of the populations in the two circular components (in either the condensate or the reservoir) then a self-induced Larmor precession of the condensate and reservoir Stokes vector occurs. Other polarization sensitivity derives from an assumed polarization splitting between states linearly polarized at  $19^\circ$  and  $109^\circ$ . This causes a rotation of the Stokes vector if the reservoir state is not an eigenstate with linear polarization of  $19^\circ$  or  $109^\circ$ , which results in non-zero  $S_3$  (Fig. 2(f)). The condensate Stokes parameters are time integrated and normalized by the time integrated condensate population for comparison to the experimental results.

The results of our model are represented by solid curves in Fig. 2. We assumed a condensate lifetime of  $2\text{ps}$ , reservoir lifetime of  $100\text{ps}$ , pulse duration of  $2\text{ps}$ ,  $\alpha_2/\alpha_1 = -0.025$ , and polarization splittings of  $50\mu\text{eV}$  for both the condensate and reservoir.  $\alpha_1$  and the strength of the self-induced Larmor precession were treated as free parameters.

In Fig. 4 we compare the FF and NF spectra for two pumping schemes, namely linear ( $\theta_p = 90^\circ$ , Fig. 4(a-b)) and left-circular (Fig. 4(c-d)) polarizations. Under linear pumping, we observe that the linewidth narrows at threshold, and luminescence is concentrated around  $k_x = 0$  and  $x = 0$ . For higher excitation power, the momentum and position distributions broaden and the condensate energy blue-shifts. Under circular pumping and at just above threshold, bottleneck condensation is observed in momentum space at  $k_x \sim \pm 2.5 \mu\text{m}^{-1}$  ( $18^\circ$  in air), while in real space luminescence is concentrated at the center of the excitation spot. This implies that scattering into the zero momentum region is only efficient when both spin species are present. For higher excitation power, luminescence is mainly observed around  $k_x = 0$  and  $x = 0$ , similar to the linear pumping case. This result is consistent with previous parametric amplification experiments [25, 26], where a suppression of the scattering rate towards the zero-momentum region was observed when only one spin species was present.

We note that the observed energy shift of the  $k_x \sim 0$  emission peak for linearly polarized pumping shows an almost logarithmic increase as a function of pumping

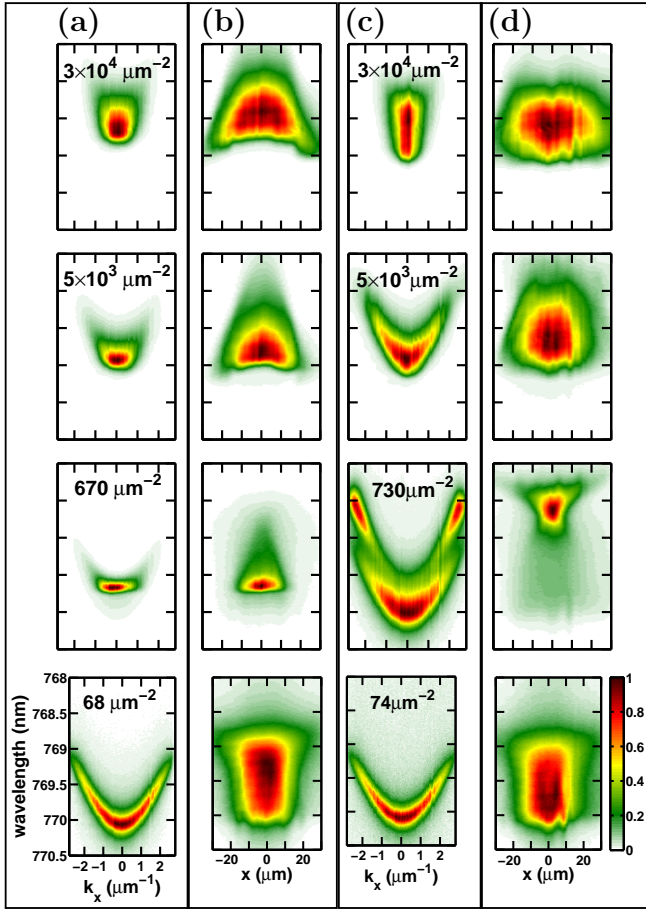


FIG. 4: (color) Far-field (FF) ( $k_x$  in  $\mu\text{m}^{-1}$  vs. wavelength in  $\text{nm}$ ) and near-field (NF) ( $x$  in  $\mu\text{m}$  vs. wavelength in  $\text{nm}$ ) spectra for various injected particle densities (in  $\mu\text{m}^{-2}$  per pulse per QW). (a) FF,  $\theta_p = 90^\circ$ ,  $\theta_d = 0^\circ$ . (b) NF, same pumping-detection scheme. (c) FF, left circular pump, right circular detection (d) NF, same pumping-detection scheme.

power, similar to Ref. [34]. From a polariton-polariton interaction point of view, a linear increase would be expected. The inefficient cooling by polariton-polariton scattering that we presented for the circular pumping case is further supported by recording the FF images (not shown here), which do not possess the  $k_y \leftrightarrow -k_y$  reflection symmetry above threshold.

In conclusion, we studied polarization-dependent luminescence from an exciton polariton system as a function of pump power and polarization in a non-resonant pumping geometry. Spin-dependent polariton-polariton interaction manifests itself in the rotation of the linear polarization axis by  $\sim 90^\circ$  under linearly polarized pumping. This can be understood in terms of a two-state model, suggesting that polaritons populate the condensate after multiple phonon scatterings and only one polariton-polariton scattering. In addition, when only one spin species is injected, we observed bottleneck condensation. This phenomenon is typically attributed to inefficient scattering, leading to photon leakage from the

cavity before polaritons relax into the zero-momentum region. Full determination of the polarization of polariton condensates reveals that the spin degree of freedom plays an important role in understanding the relaxation mechanism of microcavity exciton polaritons.

G.R. acknowledges support from JST/SORST and Special Coordination Funds for Promoting Science and Technology. T.C.H.L., Y.G.R., and A.V.K. would like to thank E.P.S.R.C. for financial support. A.V.K. thanks Ivan Shelykh for useful comments.

\* Electronic address: roumpos@stanford.edu

- [1] M. H. Anderson, et al., *Science* **269**, 198 (1995).
- [2] K. B. Davis, et al., *Phys. Rev. Lett.* **75**, 3969 (1995).
- [3] C. Weisbuch, et al., *Phys. Rev. Lett.* **69**, 3314 (1992).
- [4] Y. Yamamoto, et al., *Semiconductor Cavity Quantum Electrodynamics* (Springer-Verlag, 2000).
- [5] A. Kavokin and G. Malpuech, *Cavity Polaritons* (Academic Press, 2003).
- [6] A. Imamoglu, et al., *Phys. Rev. A* **53**, 4250 (1996).
- [7] S. Christopoulos, et al., *Phys. Rev. Lett.* **98**, 126405 (2007).
- [8] H. Deng, et al., *Proc. Natl. Acad. Sci. U.S.A.* **100**, 15318 (2003).
- [9] J. Kasprzak, et al., *Nature* **443**, 409 (2006).
- [10] H. Deng, et al., *Phys. Rev. Lett.* **99**, 126403 (2007).
- [11] H. Deng, et al., *Phys. Rev. Lett.* **97**, 146402 (2006).
- [12] F. Tassone and Y. Yamamoto, *Phys. Rev. B* **59**, 10830 (1999).
- [13] D. Porras, et al., *Phys. Rev. B* **66**, 085304 (2002).
- [14] T. D. Doan, et al., *Phys. Rev. B* **72**, 085301 (2005).
- [15] K. V. Kavokin, et al., *Phys. Rev. Lett.* **92**, 017401 (2004).
- [16] I. A. Shelykh, et al., *Phys. Stat. Solidi. b* **242**, 2271 (2005).
- [17] H. T. Cao, et al., *Phys. Rev. B* **77**, 075320 (2008).
- [18] D. N. Krizhanovskii, et al., *Phys. Rev. B* **73**, 073303 (2006).
- [19] S. Schumacher, et al., *Phys. Rev. B* **76**, 245324 (2007).
- [20] C. Ciuti, et al., *Phys. Rev. B* **58**, 7926 (1998).
- [21] P. R. Eastham and D. M. Whittaker, *Phys. Rev. B* **68**, 075324 (2003).
- [22] M. Kuwata-Gonokami, et al., *Phys. Rev. Lett.* **79**, 1341 (1997).
- [23] R. M. Stevenson, et al., *Phys. Rev. Lett.* **85**, 3680 (2000).
- [24] J. Keeling, et al., *Semicond. Sci. Technol.* **22**, R1 (2007).
- [25] A. I. Tartakovskii, et al., *Phys. Rev. B* **62**, R13298 (2000).
- [26] A. Kavokin, et al., *Phys. Rev. B* **67**, 195321 (2003).
- [27] C. W. Lai, et al., *Nature* **450**, 529 (2007).
- [28] P. Yeh, *Optical Waves in Layered Media* (John Wiley, Hoboken, 2005).
- [29] Y. Zhu, et al., *Phys. Rev. Lett.* **64**, 2499 (1990).
- [30] L. Kłopotowski, et al., *Solid State Commun.* **139**, 511 (2006).
- [31] J. Kasprzak, et al., *Phys. Rev. B* **75**, 045326 (2007).
- [32] E. Hecht, *Am. J. Phys.* **38**, 1156 (1970).
- [33] C. Leyder, et al., *Phys. Rev. Lett.* **99**, 196402 (2007).
- [34] D. Bajoni, et al., *Phys. Rev. Lett.* **100**, 047401 (2008).